



High catalytic activity of Mo–Zn–Al–O catalyst for dye degradation: Effect of pH in the impregnation process



Yang Li^a, Yin Xu^{a,*}, Xiao-ying Chen^a, Fei Ge^a, Run-liang Zhu^b

^a Department of Environmental Science and Engineering, Xiangtan University, Xiangtan, Hunan 411105, PR China

^b Guangzhou Institutes of Geochemistry, Chinese Academy of Sciences, Guangzhou 510640, PR China

ARTICLE INFO

Article history:

Received 14 March 2014

Received in revised form 28 April 2014

Accepted 6 May 2014

Available online 13 May 2014

Keywords:

Impregnation

Room conditions

Mo–Zn–Al–O catalyst

Dye wastewater

ABSTRACT

The effect of pH in the impregnation process on the phase formation, structure and catalytic potential of Mo–Zn–Al–O catalysts synthesized by the co-precipitation and impregnation method was evaluated. The materials were characterized by X-ray diffraction, UV–vis diffuse reflectance spectroscopy, Fourier transform-infrared spectroscopy, X-ray photoelectron spectroscopy and N₂ adsorption technique. The catalytic efficiency of Mo–Zn–Al–O catalysts was evaluated with respect to the degradation of cationic orchid X-BL by wet air oxidation under room conditions. The speciation diagram of Mo species in aqueous solution as a function of pH value was established. At basic pH (pH > 8), MoO₄²⁻ was the main anionic in the solution. H_nMo₇O₂₄^{m-} was formed with the decrease of pH values ranging from 8 to 4 due to the combination of H⁺ and Mo₇O₂₄⁶⁻. Molybdenum was present as solid of H₂MoO₄ when pH value was below 4.0. Interestingly, the Mo–Zn–Al–O catalyst prepared under pH = 7 has lower surface texturing values (S_{BET} = 9.9 m²/g and V_p = 0.083 cm³/g) than the Mo–Zn–Al–O catalyst prepared under pH = 4 (S_{BET} = 21.6 m²/g and V_p = 0.038 cm³/g). However, the Mo–Zn–Al–O catalysts prepared under pH = 7 shows the highest catalytic activity with 94.6% of decolorization and 86.7% of TOC removal efficiency. This highest catalytic activity can be contributed to special Mo species, special crystalline phases, tetrahedral Mo structure and highly dispersed Mo.

© 2014 Elsevier B.V. All rights reserved.

1. Introduction

Catalytic wet air oxidation (CWAO) is supposed to have a great potential for the treatment of effluent containing a high content of organic materials or toxic contaminants [1]. It has a good capacity for breaking down biologically refractory compounds to simple, which are easily treated materials, before they are released into the environment [2–4]. Hence, CWAO has been proved to be one of the most effective methods to degrade organic wastewater. Unfortunately, the CWAO process requires high temperature and high pressure, which will increase the operating costs and limit the application of the technology [5–7]. In recent years, many attempts have been made to investigate a heterogeneous catalyst such as molybdenum oxide with high activity under mild conditions [8–10].

Chemical and physical properties of the metal catalyst are generally dependent on the synthesis conditions, such as preparation methods, preparation temperature, ratios of metals, pH of the

solution and so on [11–17]. The catalytic activity of metal oxide has been influenced by the type of metal atom, the number of ligands attached to the catalyst and the nature of the remaining ligands in the coordination sphere. Therefore, very efficient and selective synthetic procedures have been reported in recent years [18–24]. In a previous paper, we have investigated the contribution of metal ratio to the catalytic activity of the Mo–Zn–Al–O catalysts and found that the Mo–Zn–Al–O catalyst with 1:1 of Zn/Al molar ratio has highest catalytic activity on the degradation of cationic red GTL. The conclusion is that the catalytic activity of Mo–Zn–Al–O catalyst depend upon the average metal–metal interatomic distance Me···Me [25]. Klimova et al. have established the diagram of Mo species in aqueous solution as a function of pH, indicating that the changes among NiMo/SBA-15 are related to the pH of the impregnation solution due to the catalyst modifications by citric acid such as morphology of active phase [26]. Therefore, we are working on synthesizing Mo–Zn–Al–O catalyst in different impregnation solution with different pH value and investigating the relationship between the physicochemical morphology of active phase on Mo–Zn–Al–O catalyst and catalytic activity in CWAO process.

In this study, the effect of pH in the impregnation process on the phase formation, structure and catalytic potential of Mo–Zn–Al–O

* Corresponding author. Tel.: +86 0731 58292231; fax: +86 0731 58292231.
E-mail address: xuyinlab@163.com (Y. Xu).

catalysts synthesized by the co-precipitation and impregnation method was evaluated. Briefly, Zn–Al LDHs was the support of the Mo–Zn–Al–O catalyst due to high surface area, pore volume and appropriate pore size for the transformation of large molecular materials [27–29]. The catalytic activities of the Mo–Zn–Al–O catalysts prepared in impregnation solution with different pH value were determined using the degradation of cationic orchid X-BL wastewater in CWAO process under room temperature and room pressure. This work is devoted to interpreting the catalytic results in terms of the pH value in impregnation process.

2. Experimental

2.1. Mo–Zn–Al–O catalyst preparation

The Mo–Zn–Al–O catalysts were prepared using the co-precipitation and impregnation method [8]. First of all, co-precipitation was used to prepare Zn–Al LDHs at pH 9.5–10 with $\text{Zn}(\text{NO}_3)_2 \cdot 6\text{H}_2\text{O}$ and $\text{Al}_2(\text{NO}_3)_3 \cdot 9\text{H}_2\text{O}$. The suspension was stirred at 70 °C for 1 h, heating and aging at 80 °C for 18 h. Then, 20 g Zn–Al LDH was added into 100 ml 0.28 mol/L ammonium heptamolybdate aqueous solution at different pH values. The select pH values in our experiment were 4–9. The impregnation solution was evaporated to dryness by water bath at 80 °C for 10 h after being kept at room temperature for 12 h. In the end, the mixture was calcined in air at 400 °C for 1 h and cooled to room temperature. We labeled the catalysts prepared under different pH values in impregnation process with Mo(4), Mo(5), Mo(6), Mo(7), Mo(8), Mo(9).

2.2. Characterization

Medusa software was used to plot the aqueous speciation diagrams of impregnation solution. To observe different species in aqueous solution, the Mo predominance area diagram was plotted for a large concentration range and the Mo fraction diagram was plotted for $[\text{Mo}(\text{VI})]_{\text{aq}} = 0.28 \text{ mol/L}$.

UV–vis diffuse reflectance spectroscopy (DRS) of the catalysts was acquired on a Japan shimadzu UV-2550 spectrophotometer where the spectra were recorded at the wavelength range of 200–800 nm.

X-ray diffraction (XRD) patterns of catalysts were recorded on a Philips Panalytical X'Pert PRO X-ray diffractometer using Cu K α radiation at 40 kV and 30 mA. The patterns were recorded in the 2θ range of 20–90° with a scan rate of 2°/min. The XRD phases present in the sample were identified with the help of the joint committee on powder diffraction standards (JCPDS) files.

Fourier transform infrared spectrometer (FT-IR) of the samples were taken within the range of 4000–400 cm^{-1} on a Nicolet Nexus-670 instrument made in USA and 2 mg of the sample mixed with 200 mg of dry KBr was pressed into a transparent disk.

The pore structure of the catalysts was analyzed by N_2 adsorption measurements on the NOVA-2000E apparatus which was made in Quantachrome Company of America. The specific surface areas were calculated by the Brunauer–Emmett–Teller (BET) method and pore volume and pore size were determined by the Brunauer–Joyner–Hallenda (BJH) method.

The X-ray photoelectron spectrometer (XPS) spectra of the catalysts were carried out on the Thermo Scientific Escalab 250 X-ray spectrometer made in Britain. The Al K α excitation source was at 1486.7 eV, with a voltage of 15 kV and an emission current of 10 mA. The kinetic energy of photoelectrons was measured using a hemispherical electrostatic analyzer working in a constant pass energy mode. The charging effect of the sample was corrected by referring to the C 1s peak of contaminant carbon (binding energy (BE) = 284.6 eV).

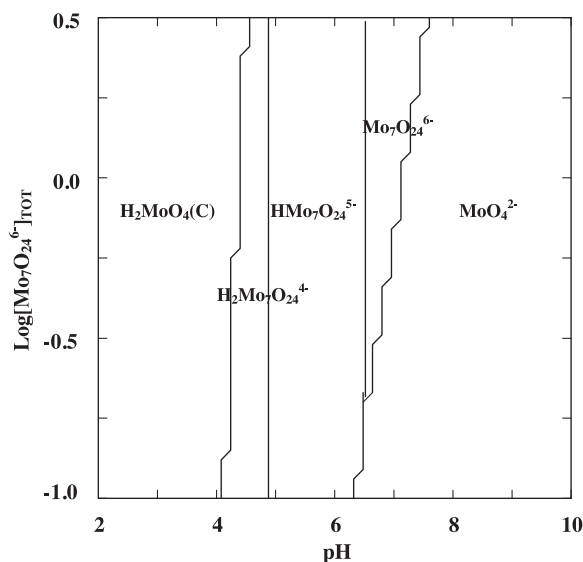


Fig. 1. Predominance area diagrams for aqueous solution of Mo.

2.3. Catalytic activity measurements

The catalytic activity of Mo–Zn–Al–O catalysts was determined by the wet air catalytic oxidation of 100 mg/L cationic orchid X-BL corresponding to 640 times of chromaticity under room temperature and atmospheric pressure. The Mo–Zn–Al–O catalyst with 1 g was used to degrade a 1 L solution of cationic orchid X-BL with concentration of 100 mg/L. The solution was aerated by the silver lake SP-780 aeration equipment with a rate of 3.5 L/min. The pH of the operating solution was not adjusted in the whole CWAO process. The decomposition rate of cationic orchid X-BL was estimated on the basis of the absorbency by UV–vis spectrophotometer (Japan shimadzu UV 2550) and TOC analyzer (Japan shimadzu CPH CN200).

3. Results and discussion

3.1. Compounds in aqueous solution

Fig. 1 shows the speciation diagram for Mo(VI) species present in aqueous solution at different pH values. As described in the previous paper [26], the type and dispersion of Mo species was present in aqueous solution of different Mo concentrations changed with the pH value. From Fig. 1, at basic pH (pH > 8), MoO_4^{2-} was the main anionic in the solution. Heptamolybdate was predominant when pH value was between 8 and 4. $\text{H}_7\text{Mo}_7\text{O}_{24}^{m-}$ was formed with the decrease of pH values due to the combination of H^+ and $\text{Mo}_7\text{O}_{24}^{6-}$. Molybdenum was present as a solid of H_2MoO_4 when pH value was below 4.0. In this work, the impregnation solution with ammonium heptamolybdate concentration of 0.28 mol/L, which corresponds to the $\log[\text{Mo}_7\text{O}_{24}^{6-}] = -0.55$. The percentage of molybdenum compounds existed in the impregnation solution at different pH values is shown in Fig. 2. Mixtures of $\text{H}_2\text{Mo}_7\text{O}_{24}^{4-}$, $\text{HMo}_7\text{O}_{24}^{5-}$, $\text{Mo}_7\text{O}_{24}^{6-}$ and MoO_4^{2-} are formed at pH value between 4.0 and 9.0. As the increase of the pH values, $\text{Mo}_7\text{O}_{24}^{6-}$ anionic where Mo is in octahedral symmetry gradually transfers into MoO_4^{2-} where Mo is in tetrahedral symmetry. Associated Fig. 1 with Fig. 2, Mo anionic entirely formed the solid of H_2MoO_4 at the pH value of 4.0. The fraction of $\text{HMo}_7\text{O}_{24}^{5-}$ was 0.62 and 0.68 under pH = 5.0 and pH = 6.0 which demonstrated $\text{HMo}_7\text{O}_{24}^{5-}$ is the dominant species. When the pH value was 7, the fraction of $\text{Mo}_7\text{O}_{24}^{6-}$ and MoO_4^{2-} was 0.42 and 0.48. A small part of Mo was transferred into $\text{Mo}_7\text{O}_{24}^{6-}$ and

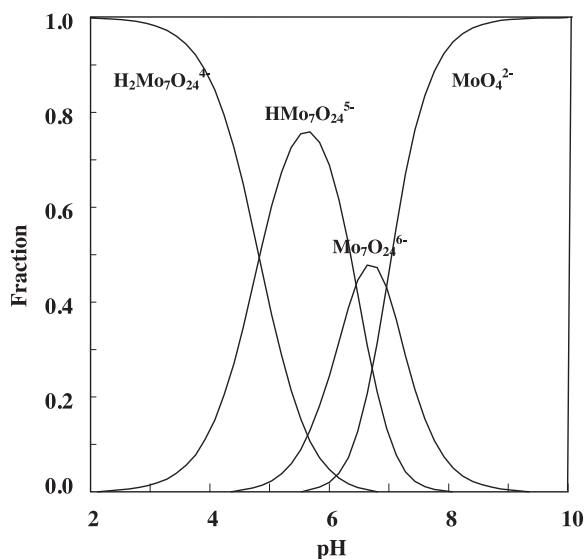


Fig. 2. Fraction diagram of aqueous solution of Mo.

the most converted into MoO_4^{2-} at $\text{pH} = 8$. The species of MoO_4^{2-} was the only species when the pH was 9.

3.2. Structural characteristics of Mo–Zn–Al–O catalysts

3.2.1. XRD investigation

Fig. 3 indicates the XRD patterns of Mo–Zn–Al–O catalysts prepared by wet impregnation method at different pH values. All the catalysts exhibited a well crystallized pattern. The patterns of Mo(4), Mo(5) and Mo(6) demonstrates the typical diffraction peaks of MoO_3 (JCPDS 35-0609) phase at $2\theta = 23.3^\circ$, 25.7° and 27.3° . Furthermore, the intensity of this typical diffraction peak was decreased with the increase of pH values, suggesting a decrease in the crystallinity size of MoO_3 . Interestingly, when the pH increased by adding NaOH , a mixture of polymolybdate such as Na_2MoO_4 , $\text{Na}_2\text{Mo}_4\text{O}_{13}$ and $\text{Na}_2\text{Mo}_2\text{O}_7$ phases was observed in the patterns of Mo(7) and Mo(8). The main diffraction patterns of 2θ at 25.7° , 26.1° and 30.5° were the characteristic diffraction peaks of $\text{Na}_2\text{Mo}_4\text{O}_{13}$ phase. Very small line at $2\theta = 23.5^\circ$, 27.6° , 28.3° , 28.5° and 29.1° have also been ascribed to the phase of $\text{Na}_2\text{Mo}_2\text{O}_7$. When the pH increased to 9, these mixtures of polymolybdate phase suddenly vanish and the tall and thin peaks were attributed to Na_2MoO_4

(JCPDS 12-0773). For Na_2MoO_4 , the main characteristic diffraction peak of 2θ value was 27.6° , 32.6° , 48.9° , 52.1° and 57.1° . This structure change is well in line with the results of Figs. 1 and 2.

3.2.2. FT-IR investigation

The results of FT-IR spectra are illustrated in Fig. 4. A major peak at 3425 cm^{-1} represents in all the FT-IR spectra due to stretching of hydroxide radical. In the fingerprint region range from 1618 cm^{-1} to 1634 cm^{-1} , it shows a sharp band which is mainly assigned to stretching vibration of Na-O-Mo . The stretching of Al-O is found at 1384 cm^{-1} . From Fig. 4b, a few differences occur with the prepared catalysts ranging from 400 cm^{-1} to 1000 cm^{-1} . The band at 990 cm^{-1} is ascribed to the stretching modes of the Mo=O terminal bond presented in each octahedron of MoO_3 in Mo(4), Mo(5) and Mo(6) which was in accord with the XRD results. The peaks at 870 cm^{-1} and 750 cm^{-1} caused by the stretching vibrations of bridging Mo-O and O-Mo-O confirm the assignment concerning the Na-Mo-O formation [25]. The broadness of the 870 cm^{-1} band in Mo(6), Mo(7) and Mo(8) explains that there was not completely pure probably due to different crystal phase. The FT-IR of Mo(9) presented typical bands at 840 cm^{-1} , 750 cm^{-1} and 560 cm^{-1} in conformity with XRD results validating the formation of Na_2MoO_4 .

3.2.3. Optical absorption property

The optical absorption property of the catalyst has been recognized as the key factor in affecting its catalytic performance. Fig. 5 illustrates the UV–vis DRS of Mo–Zn–Al–O catalysts. In the 200–400 nm region, the different absorptions are associated to charge transfer transitions ($\text{O}_2-\text{Mo}^{6+}$) from the O_{2p} valence bands of the supported oxides to the Mo 3d orbital distanced to the bulk individual oxides [30]. A wide band was found in the UV–vis DRS of Mo(4), Mo(5) and Mo(6). This wide band can be divided into two peaks. One was concentrated at about 244 nm, which is assigned to the tetrahedral Mo. The other appeared at about 305 nm is attributed to the octahedral Mo [31]. Both octahedral Mo and tetrahedral Mo species were present in MoO_3 crystal which is confirmed by the XRD results. The spectra of Mo(7), Mo(8) and Mo(9) was a little different. Take Mo(7) for example, the band at 270–400 nm was steep and there was no peak at 305 nm. That is to say, the metal-oxide centers are different with the increase of pH value. An electronic interaction between oxide-surface species occur through oxygen bridging of the polyhedral structure, facilitated by a lower equivalent overall coordination [32]. This phenomenon is similar

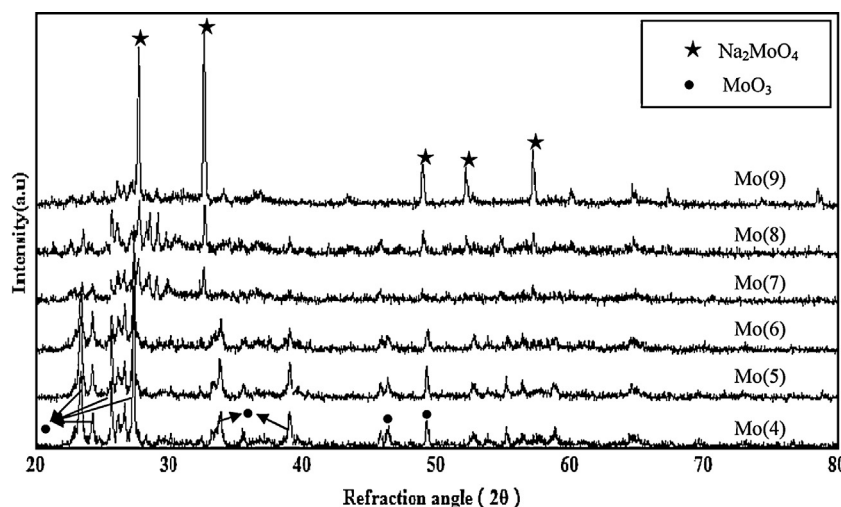


Fig. 3. XRD patterns of Mo–Zn–Al–O catalysts at different impregnation values.

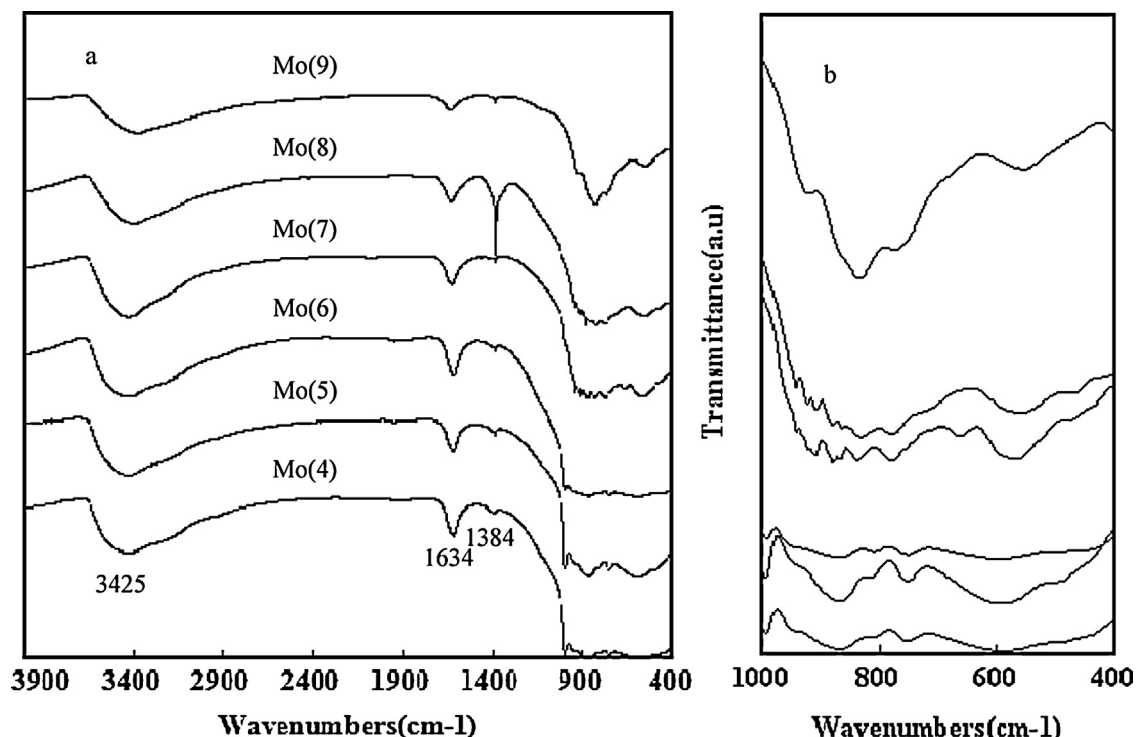


Fig. 4. FT-IR spectra of Mo-Zn-Al-O catalysts at different impregnation values.

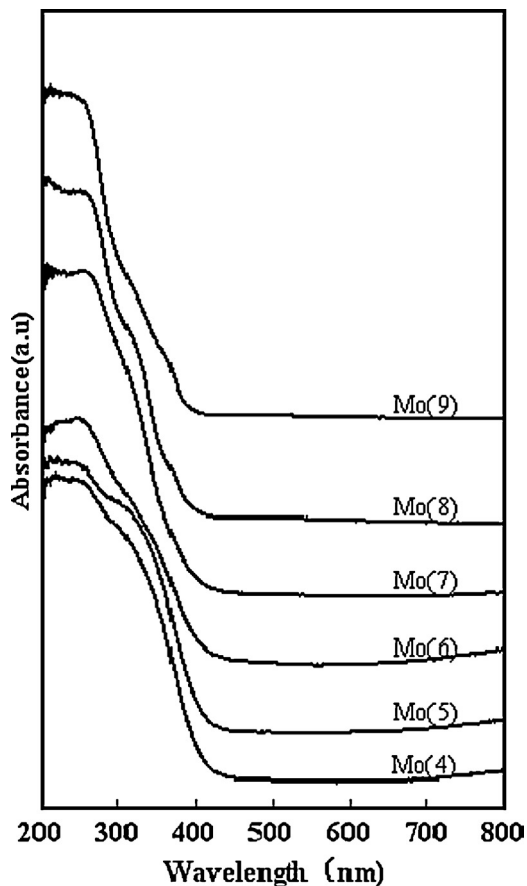


Fig. 5. Ultraviolet–visible absorbance spectra of Mo-Zn-Al-O catalysts at different impregnation values.

to the result of Mo species in different pH value and XRD patterns of different Mo-Zn-Al-O catalysts.

3.2.4. XPS analysis

The surface composition and chemical states were further analyzed by XPS based on the characteristic binding energies of different elements on material surface. The XPS spectra of Mo-Zn-Al-O catalysts are shown in Fig. 6. The binding energy for C 1s peak at 284.6 eV was used as the reference for calibration. In the full spectrum of XPS, the strength of Na 1s and Zn LMM spectra became stronger with the increase of the pH value. It is clear that NaOH was used in our work to adjust the pH of the impregnation aqueous solution. So, the increase of Na content is not a surprise. Chemical compositions obtained by XPS spectra of the prepared Mo-Zn-Al-O catalysts are listed in Table 1. Notably, the fact that the percentage of Mo dosing in the catalysts was a similar value in all catalysts indicates that the catalytic activity is not affected by content of Mo.

Fig. 7 shows the spectra of Mo $3d_{3/2}$ and $3d_{5/2}$ of the catalysts. The binding energies of all samples exhibited the presence of a double peak structure and the space between the two peaks was in agreement with an early reported value of 3.2 eV [33]. All Mo $3d_{3/2}$ and $3d_{5/2}$ peaks were sharp, demonstrating that Mo exists mainly

Table 1
Chemical compositions obtained by XPS spectra of the prepared Mo-Zn-Al-O catalysts.

| Catalysts | Mo (at%) | Na (at%) | Zn (at%) | Al (at%) | C (at%) | O (at%) |
|-----------|----------|----------|----------|----------|---------|---------|
| Mo(4) | 15.549 | 1.213 | 1.958 | 19.487 | 14.7 | 47.093 |
| Mo(5) | 15.939 | 1.214 | 1.771 | 19.002 | 18.382 | 43.693 |
| Mo(6) | 12.586 | 1.322 | 3.402 | 5.16 | 28.775 | 48.754 |
| Mo(7) | 10.98 | 4.253 | 2.072 | 23.502 | 17.263 | 41.93 |
| Mo(8) | 13.882 | 6.269 | 3.467 | 4.576 | 19.98 | 51.825 |
| Mo(9) | 13.867 | 11.223 | 2.923 | 2.339 | 18.059 | 51.589 |

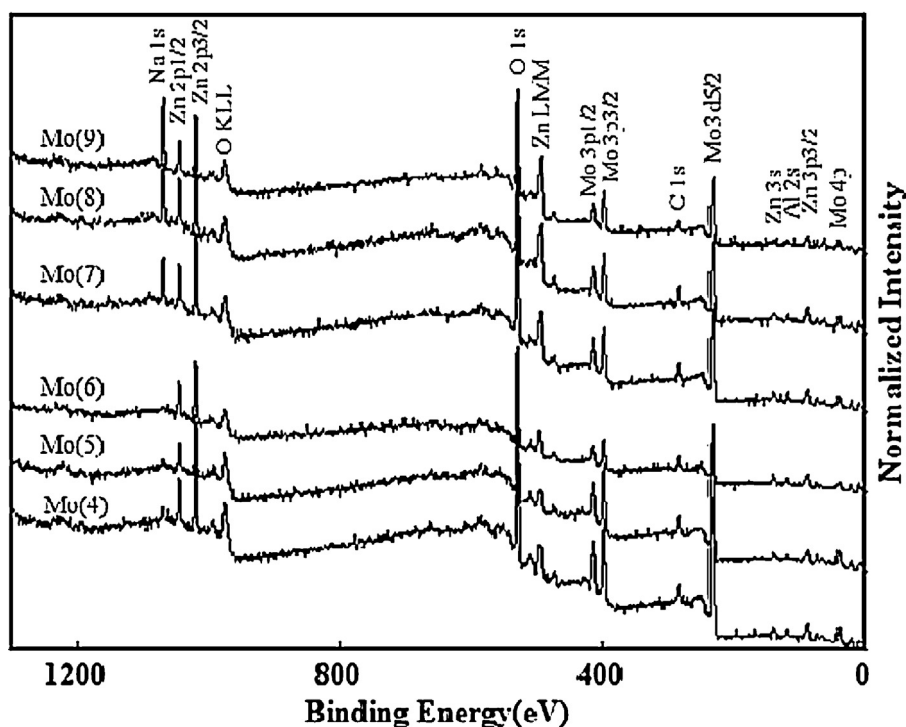


Fig. 6. The full spectrum of XPS of Mo–Zn–Al–O catalysts at different impregnation values.

in the form of Mo^{6+} on catalyst surface. The MoO_3 reference spectrum has a peak at about 232.8 eV and 235.9 eV which was found in the spectra of Mo(4) sample. Compared with Mo(4), the shift of Mo 3d to lower BE is related to the presence of Mo^{6+} existence depending on the pH value in the preparation of the Mo–Zn–Al–O catalyst. This shift movement of 0.2–0.5 eV indicates the catalyst transfers from MoO_3 into Na_2MoO_4 with the increase of pH value [34,35].

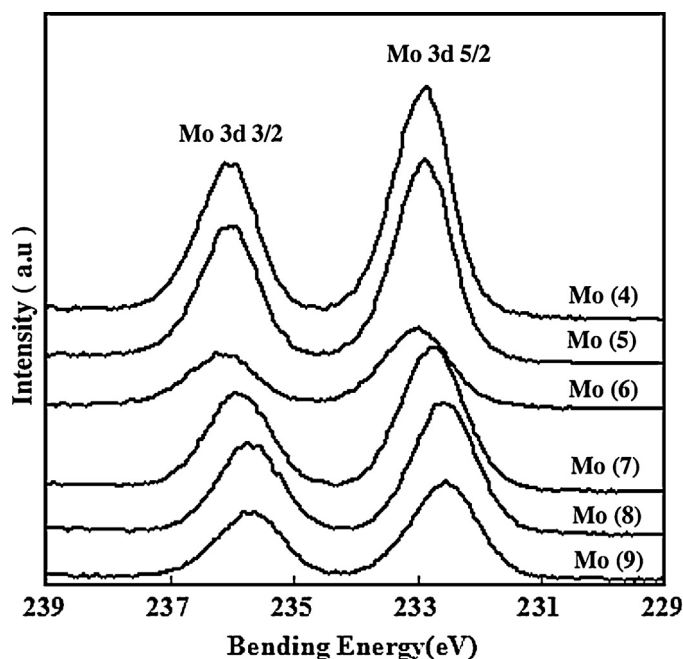


Fig. 7. Mo 3d_{3/2} and 3d_{5/2} peaks of XPS of Mo–Zn–Al–O catalysts at different impregnation values.

3.2.5. Surface texturing properties

The porous structures of all prepared catalysts were determined by N_2 adsorption–desorption isotherm method. As illustrated in Fig. 8, a type IV with an obvious H3 hysteresis loop ($P/P_0 < 0.4$) according to IUPAC classification was present, indicating the presence of mesoporous. H3 hysteresis loop is commonly attributed to slit-shape pore generated of plate-like particles. In addition, though isotherms for all samples are quite similar, there is difference in surface area, pore volume and pore diameter (Table 2). Interestingly, the Mo–Zn–Al–O catalyst prepared by wet impregnation method at pH = 7 indicates lower surface texturing values ($S_{\text{BET}} = 9.9 \text{ m}^2/\text{g}$ and $V_p = 0.083 \text{ cm}^3/\text{g}$) than the Mo–Zn–Al–O catalyst prepared under pH = 4 ($S_{\text{BET}} = 21.6 \text{ m}^2/\text{g}$ and $V_p = 0.038 \text{ cm}^3/\text{g}$). This indicates that the catalytic activity was not affected by surface area of the catalyst.

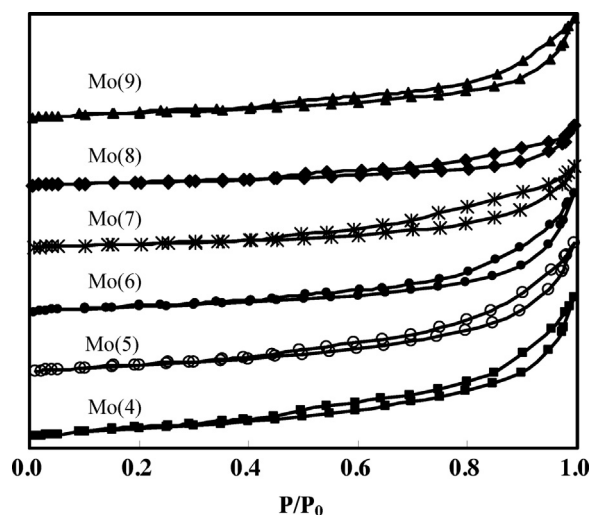


Fig. 8. N_2 adsorption–desorption isotherm curve of Mo–Zn–Al–O catalysts.

Table 2

The surface area, pore volume and pore diameter for the prepared Mo–Zn–Al–O catalysts.

| Catalysts | Impregnation pH | Specific area (m ² /g) | Pore volume (cm ³ /g) | Pore diameter (nm) |
|-----------|-----------------|-----------------------------------|----------------------------------|--------------------|
| Mo(4) | 4 | 21.6 | 0.083 | 3.78 |
| Mo(5) | 5 | 22.6 | 0.077 | 3.77 |
| Mo(6) | 6 | 16.6 | 0.081 | 3.82 |
| Mo(7) | 7 | 11.8 | 0.047 | 3.78 |
| Mo(8) | 8 | 9.9 | 0.038 | 3.83 |
| Mo(9) | 9 | 14.8 | 0.055 | 3.78 |

3.3. Catalytic activities of Mo–Zn–Al–O catalysts in CWAO of cationic orchid X-BL under room conditions

Fig. 9 shows the catalytic activity of prepared Mo–Zn–Al–O catalysts on the decoloration and TOC removal efficiency of cationic orchid X-BL under room conditions. It shows that the pH value in impregnation process has a powerful influence on the CWAO

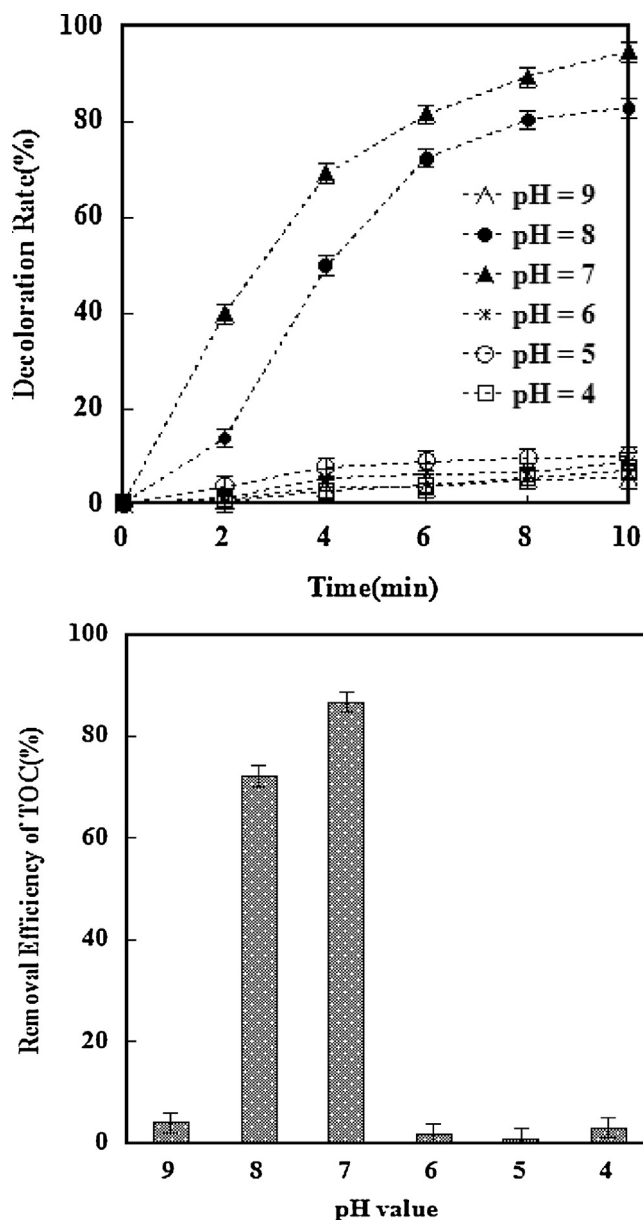


Fig. 9. The decoloration and TOC removal efficiency of cationic orchid X-BL by Mo–Zn–Al–O catalysts prepared at different impregnation values in CWAO process.

Table 3

The leaching rate of Mo after CWAO reaction by the prepared Mo–Zn–Al–O catalysts.

| Catalysis | Mo(4) | Mo(5) | Mo(6) | Mo(7) | Mo(8) | Mo(9) |
|-----------------------|--------|--------|-------|-------|--------|--------|
| Leaching amount (g/g) | 0.0042 | 0.0038 | 0.004 | 0.015 | 0.0184 | 0.0261 |

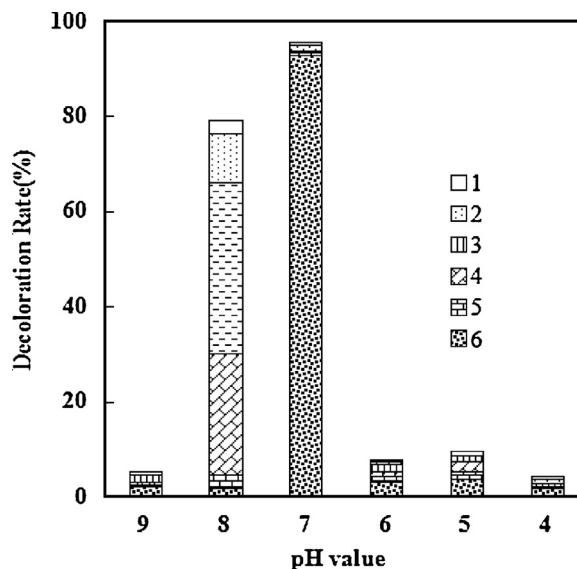


Fig. 10. The reproducibility of Mo–Zn–Al–O catalysts prepared with different pH value in the impregnation process.

activity of Mo–Zn–Al–O catalysts. The catalysts of Mo(7) and Mo(8) shows a good catalytic activity on the degradation of cationic orchid X-BL under room conditions. However, the other catalysts have barely removal efficiency. The Mo–Zn–Al–O catalysts prepared under pH=7 showed the highest catalytic activity with 94.6% of decolorization and 86.7% of TOC removal efficiency. In order to investigate the economic and practice property of these catalysts, the leaching rate of Mo is tested after the reaction which is shown in the Table 3. In our system, the fact that the leaching rate of Mo increased with the increase of pH value indicates that Mo species in the catalyst is from Mo-oxide to molybdate in the preparation process. The reproducibility is a more important parameter for the evaluating the stability of a catalyst. The catalytic runs in CWAO process by Mo–Zn–Al–O catalysts prepared under different pH value in impregnation process are shown in Fig. 10. The result indicates that the color removal efficiency by the Mo–Zn–Al–O catalysts prepared under pH=7 after six recycling runs experimental cycles remained as the same as the first experiment.

4. Conclusion

In the present work, a series of Mo catalysts supported on Zn–Al LDHs were prepared by wet impregnation method at different pH values. The pH value in the impregnation solution has a great effect on the catalytic activity of Mo–Zn–Al–O catalysts in CWAO process at room temperature and atmospheric pressure. Of particular interest, the existence of Mo species in the catalyst affected the surface, crystal and morphological properties of the prepared catalysts. It can be concluded that the optimum pH value in the impregnation process of Mo–Zn–Al–O catalysts was 7 for the degradation of the cationic orchid X-BL. This highest catalytic activity can be contributed to special Mo species, special crystalline phases, tetrahedral Mo structure and highly dispersed Mo.

Acknowledgments

We gratefully acknowledge the financial support from the Research Foundation of National Natural Science Foundation of China (No. 51308484), Research Foundation of Natural Science Foundation of Hunan Province (No. 13JJ4049) and Specialized Research Fund for the Doctoral Program of Xiangtan University (No. 12QDZ18).

References

- [1] D.B. Akolekar, S.K. Bhargava, I. Shirgoankar, J. Prasad, Appl. Catal. A 236 (2002) 255–262.
- [2] F. Arena, C. Italiano, G. Drago Ferrante, G. Trunfio, L. Spadaro, Appl. Catal. B 144 (2014) 292–299.
- [3] F. Arena, J. Negro, A. Parmaliana, L. Spadaro, G. Trunfio, Ind. Eng. Chem. Res. 46 (2007) 6724–6731.
- [4] B. Erjavec, R. Kaplan, P. Djinovic, A. Pintar, Appl. Catal. B 132–133 (2013) 342–352.
- [5] K.-H. Kim, S.-K. Ihm, J. Hazard. Mater. 186 (2011) 16–34.
- [6] J. Levec, A. Pintar, Catal. Today 124 (2007) 172–184.
- [7] J.-M. Wu, W. Wen, Environ. Sci. Technol. 44 (2010) 9123–9127.
- [8] Y. Xu, X. Li, X. Cheng, D. Sun, X. Wang, Environ. Sci. Technol. 46 (2012) 2856–2863.
- [9] Y. Zhang, D. Li, Y. Chen, X. Wang, S. Wang, Appl. Catal. B 86 (2009) 182–189.
- [10] S. Zhao, X. Wang, M. Huo, Appl. Catal. B 97 (2010) 127–134.
- [11] G.R. Bamwenda, S. Tsubota, T. Nakamura, M. Haruta, Catal. Lett. 44 (1997) 83–87.
- [12] A. Bienholz, F. Schwab, P. Claus, Green Chem. 12 (2010) 290–295.
- [13] C. Cao, G. Yang, L. Dubau, F. Maillard, S.D. Lambert, J.-P. Pirard, N. Job, Appl. Catal. B 150 (2014) 101–106.
- [14] P. Maki-Arvela, D.Y. Murzin, Appl. Catal. A 31 (2013) 251–281.
- [15] C. Fountzoula, N. Spanos, H.K. Matralis, C. Kordulis, Appl. Catal. B 35 (2002) 295–304.
- [16] A. Kambur, G.S. Pozan, I. Boz, Appl. Catal. B 115–116 (2012) 149–158.
- [17] R.Q. Long, R.T. Yang, Catal. Lett. 74 (2001) 201–205.
- [18] M. Houalla, C.L. Kibby, L. Petrakis, D.M. Hercules, J. Catal. 83 (1983) 50–60.
- [19] A.O. Jackson, B.A. Larkins, Plant Physiol. 57 (1976) 5–10.
- [20] D.H. Kim, S.I. Woo, O. Yang, Appl. Catal. B 26 (2000) 285–289.
- [21] A. Lekhal, B.J. Glasser, J.G. Khinast, Chem. Eng. Sci. 59 (2004) 1063–1077.
- [22] F. Moreau, G.C. Bond, A.O. Taylor, J. Catal. 231 (2005) 105–114.
- [23] G. Ovejero, A. Rodriguez, A. Vallet, S. Willerich, J. Garcia, Appl. Catal. B 111 (2012) 586–594.
- [24] S. Kasztelan, J. Grimblot, J.P. Bonnelle, E. Payen, H. Toulhoat, Y. Jacquin, Appl. Catal. 7 (1983) 91–112.
- [25] Y. Xu, D. Sun, Chem. Eng. J. 183 (2012) 332–338.
- [26] T.E. Klimova, D. Valencia, J.A. Mendoza-Nieto, P. Hernandez-Hipolito, J. Catal. 304 (2013) 29–46.
- [27] F. Cavani, F. Trifiro, A. Vaccari, Catal. Today 11 (1991) 173–301.
- [28] K.-H. Goh, T.-T. Lim, Z. Dong, Water Res. 42 (2008) 1343–1368.
- [29] Q. Wang, D. O'Hare, Chem. Rev. 112 (2012) 4124–4155.
- [30] M.O. Guerrero-Perez, M.C. Herrera, I. Malpartida, M.A. Larrubia, L.J. Alemany, Catal. Today 118 (2006) 360–365.
- [31] A. Duan, G. Wan, Z. Zhao, C. Xu, Y. Zheng, Y. Zhang, T. Dou, X. Bao, K. Chung, Catal. Today 119 (2007) 13–18.
- [32] M.A. Larrubia, G. Busca, Mater. Chem. Phys. 72 (2001) 337–346.
- [33] B.S. Liu, L. Jiang, H. Sun, C.T. Au, Appl. Surf. Sci. 253 (2007) 5092–5100.
- [34] S. Al-Kandari, H. Al-Kandari, A.M. Mohamed, F. Al-Kharafi, A. Katrib, Appl. Catal. A 475 (2014) 497–502.
- [35] M. Yuan, S. Wang, X. Wang, L. Zhao, T. Hao, Appl. Surf. Sci. 257 (2011) 7913–7919.